

Bonding and Structure of Ceramic-Ceramic Interfaces

Kohei Shimamura,^{1,2,3} Fuyuki Shimojo,^{1,2} Rajiv K. Kalia,¹ Aiichiro Nakano,¹ and Priya Vashishta¹

¹*Collaboratory for Advanced Computing and Simulations, Department of Physics and Astronomy, Department of Computer Science, Department of Chemical Engineering and Materials Science, University of Southern California, Los Angeles, California 90089-0242, USA*

²*Department of Physics, Kumamoto University, Kumamoto 860-8555, Japan*

³*Department of Applied Quantum Physics and Nuclear Engineering, Kyushu University, Fukuoka 819-0395, Japan*

(Received 17 March 2013; published 8 August 2013)

Quantum molecular dynamics simulations of α -Al₂O₃(0001)/3C-SiC(111) interfaces reveal profound effects of thermal annealing for producing strong interfaces consisting solely of cation-anion bonds and their consequence on interfacial structures. A Si-terminated SiC surface and Al₂O₃ form a stronger interface (Si-interface) with a Si-O bond density of 12.2 nm⁻², whereas the C interface has an Al-C bond density of 9.46 nm⁻². The interfacial bond strengthening is accompanied by the formation of an Al₂O₃ interphase with a thickness of 2–8 Å. Such atomistic understanding may help rational interfacial design of high-temperature ceramic composites for broad applications such as power generation systems.

DOI: [10.1103/PhysRevLett.111.066103](https://doi.org/10.1103/PhysRevLett.111.066103)

PACS numbers: 68.35.-p, 02.70.Ns, 71.15.Pd, 81.05.Je

Interfaces in multicomponent material systems essentially determine material behaviors [1]. Recent advancements in experimental techniques have renewed interest in atomistic structures of ceramic-ceramic interfaces. For example, x-ray computed microscopy utilizing high-flux synchrotron sources resolved interfacial debonding and sliding *in situ* during the cracking of ceramic matrix composites at high temperatures [2]. Such microscopic knowledge has significant implications for the understanding of damage mechanisms in next-generation gas turbines and hypersonic-flight applications. Moreover, high-resolution transmission electron microscopy (HRTEM) identified rich interfacial phases of thickness ~ 10 Å, which have distinct atomistic structures that do not exist in bulk phases [3,4]. These interphases [5] (or complexions [3,4]) play a decisive role in determining material properties of ceramics.

An archetypal ceramic-ceramic interface is formed between alumina (Al₂O₃) and silicon carbide (SiC), which is important for broad applications such as matrix-nanoparticle composites [6,7] and high-power electronic devices [8]. An emerging application is self-healing nanocomposites that autonomously heal cracks and recover strengths at high service temperatures in their applications such as turbines in power generators [9]. Though structural and thermo-mechanical properties of Al₂O₃ [10–12] and SiC [5,13,14] on their own have been studied intensively, those of Al₂O₃/SiC interfaces remain poorly understood. HRTEM revealed the existence of thin amorphous layers at Al₂O₃/SiC interfaces in ceramic nanocomposites [6]. The existence of such intergranular glass phases had been predicted theoretically [15]. For better understanding and design of Al₂O₃/SiC interfaces, the central question is what is the nature of interfacial bonding at the atomistic level and its consequence on interphase structures?

Unfortunately, construction of an atomic structure model for Al₂O₃/SiC interfaces has been prohibitive partly due to the large lattice mismatch between the crystal structures of Al₂O₃ and SiC. For example, the α -Al₂O₃(0001)/3C SiC(111) interface has 35% lattice mismatch. Thus, the challenge is to develop an atomistic interfacial model, on which interfacial bonding properties and interphase structures can be systematically studied. This will require high-temperature quantum molecular dynamics (QMD) simulations to obtain a well-ordered interfacial structure by thermal annealing, in which interatomic forces are computed quantum mechanically [16]. Here, high-temperature QMD simulations of α -Al₂O₃(0001)/3C-SiC(111) interfaces reveal the formation of stronger and well-ordered interfaces consisting solely of cation-anion bonds by thermal annealing. The interfacial bond strengthening is accompanied by the formation of an Al₂O₃ interphase with thickness of 2–8 Å.

In our QMD simulations, the electronic states are calculated using the projector-augmented-wave method [17,18], which is an all-electron electronic-structure-calculation method within the frozen-core approximation. In the framework of density functional theory, the generalized gradient approximation [19] is used for the exchange-correlation energy with nonlinear core corrections [20]. The momentum-space formalism is utilized [21], where the plane-wave cutoff energies are 30 and 250 Ry for the electronic pseudowave functions and the pseudocharge density, respectively. The energy functional is minimized iteratively using a preconditioned conjugate-gradient method [22,23]. Projector functions are generated for the 3s, 3p, and 3d states of Al and Si and the 2s and 2p states of C and O.

The electronic-structure-calculation code has been implemented on parallel computers [23] by a hybrid

approach combining spatial decomposition (i.e., distributing real-space or reciprocal-space grid points among processors) and band decomposition (i.e., assigning the calculations of different Kohn-Sham orbitals to different processors). The program has been implemented using the message passing interface (MPI) library for interprocessor communications.

QMD simulations are carried out using interatomic forces that are computed quantum mechanically based on the Hellmann-Feynman theorem. The equations of motion are integrated numerically with a time step of 100 a.u. (~ 2.4 fs). The initial configuration consists of hexagonal crystalline unit cells of Al-terminated α -Al₂O₃ (0001) repeated two-by-two in the lateral (a -axis) directions, which is stacked along the c axis with a slab of three-by-three lateral crystalline unit cells of 3C SiC (111); see Fig. 1. Periodic boundary conditions are applied in all directions. This makes two interfaces, where C or Si atoms face Al in the top or bottom interfaces, respectively. Hereafter, the top and bottom interfaces are called C interface and Si interface, respectively. This interfacial configuration has a lattice mismatch of 3%. Two different system sizes are simulated to assess the size effect: 174 atoms (24Al₂O₃ + 27SiC) with the simulation box size $L_z = 22.0$ Å; and 348 atoms (48Al₂O₃ + 54SiC) with $L_z = 42.0$ Å (see Fig. S1 in the Supplemental Material [24]). The lateral size of the hexagonal simulation box, $L_x = 9.2449$ Å, is the same for the two systems. In order to mimic the infinite substrate height in the SiC side (as in the case of atomic layer deposition of an Al₂O₃ layer on a hexagonal SiC substrate [8]), the atomic positions of the central Si-C bilayer are kept fixed during the simulations. In both systems, the Γ point is used for Brillouin zone sampling for electronic structure calculation.

Starting from the initial configuration, we first relax the atomic positions using a quasi-Newton method to obtain a local minimum energy configuration closest to the initial configuration. This may correspond to experimental interfaces obtained by low-temperature deposition, though

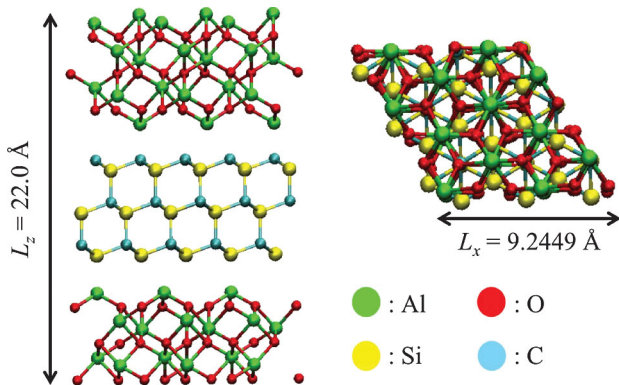


FIG. 1 (color). Side (left) and top (right) views of the initial configuration, where green, red, yellow, and cyan spheres represent Al, O, Si, and C atoms, respectively.

kinetic effects during growth are beyond the scope of this Letter. Figure 2(b) shows the relaxed interfacial structure. At both top and bottom interfaces, O atoms are displaced from the Al₂O₃ toward the SiC side to form O-C bonds (at the C-interface) and O-Si bonds (at the Si-interface), respectively. In addition, there are Al-C and Al-Si bonds, at the C- and Si-interfaces, respectively.

We also calculate atomic charges using the Mulliken bond-overlap population (BOP) analysis [24]. Figure 2(a) shows the atomic charges as a function of the atomic position in the z direction. We see charge transfer mainly from Al to Si. We have also relaxed the initial configuration of the larger system (nearly doubling the height) and found that the size effect is negligible for the atomic structures and charges (see Fig. S2 in the Supplemental Material [24]).

We next anneal the interfacial structures thermally by a melt-quench procedure. We perform a sequence of QMD simulations in the canonical ensemble at temperatures of 600, 900, 1200, 1500, 2000 and 2500 K. At each temperature, the simulation is run for 2.4 ps (1000 steps). The Al₂O₃ melts during the 2500 K simulation (the experimental

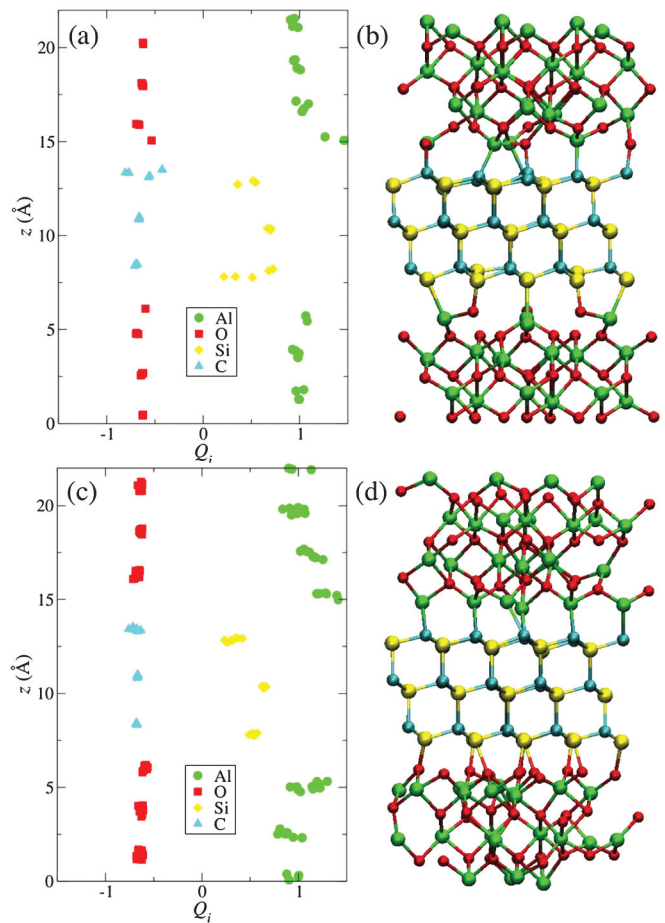


FIG. 2 (color). Charge profile (a) and atomic configuration (b) after the structural relaxation of the initial configuration. Charge profile (c) and atomic configuration (d) of the annealed structure.

melting temperature of Al_2O_3 is 2330 K [12]), while SiC remains in the solid phase (the experimental decomposition temperature of SiC is 3250 K [14]). After thermalization at 2500 K for 2.4 ps, the temperature is gradually lowered to 300 K in 2.4 ps. Finally the atomic positions are relaxed to obtain the minimum energy configuration for the annealed structure using a quasi-Newton method.

The annealed interfacial structures are shown in Fig. 2(d), which exhibit a drastic change of the structure and bonding. At the C interface, Al atoms are displaced toward the top C layer to form an interface that consists solely of Al-C bonds. On the other hand, at the Si interface, O atoms are displaced toward the bottom Si layer to form an interface that consists solely of Si-O bonds. In short, the annealing has produced more ordered layered structures at both C and Si interfaces, where only cation-anion bonds (i.e., Al-C and Si-O, respectively, at the C and Si interfaces) exist. This is in contrast to mixed interfacial bonding in the relaxed initial configuration, where cation-cation (Al-Si) and anion-anion (O-C) bond coexist with cation-anion bonds. The Cartesian coordinates of all the atoms in the annealed configuration are given in the Supplemental Material [24].

The atomic charges of the annealed configuration are plotted in Fig. 2(c). We see that Al atoms near the interfaces are more positively charged than the Al atoms in bulk Al_2O_3 , while Si and C acquire slightly negative charges compared to the bulk SiC values. Namely, charge transfer occurs from Al to Si and C. In contrast, interfacial O atoms have nearly the same charges as in bulk Al_2O_3 . As shown in Fig. 2(a), the atomic charges of C and Si atoms at the interface are rather scattered before annealing, reflecting the coexistence of various bonds. After annealing, they become less scattered, reflecting the ordering of the interfacial bonds. On the other hand, the atomic charges of Al atoms are more scattered after annealing, indicating that structural changes in the Al_2O_3 interphase accompany the interfacial bond changes.

The “purification” of the interfacial bonds (i.e., elimination of cation-cation and anion-anion bonds) described above is summarized in Fig. 3 using the Mulliken BOP analysis [24]. The figure compares the total BOP summed over all interfacial bonds per surface unit cell between the

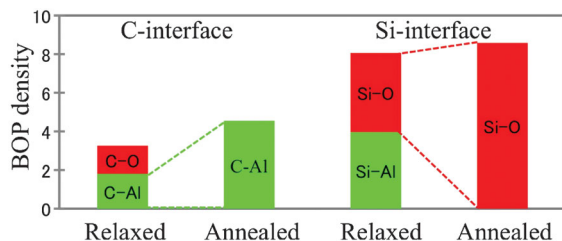


FIG. 3 (color). Purification and strengthening of interfacial bonds by annealing. Total bond overlap populations (per interfacial unit cell) of the C and Si interfaces are shown for both relaxed and annealed configurations. Red and green colors denote bonds containing O and Al, respectively.

relaxed initial and annealed configurations at both C and Si interfaces. Interfacial bond purification is reflected by the disappearance of BOP contributions arising from C-O (red) and Si-Al (green) bonds at the C and Si interfaces, respectively, after annealing. Also, the total BOP increases, signifying the strengthening of interfacial bonding, due to annealing at both interfaces. We also note that the Si interface has a larger BOP density than the C interface, showing that the Si-terminated 3C SiC (111) surface forms a stronger bonding with Al_2O_3 than the C-terminated surface. Namely, the BOP density per interfacial unit cell is 8.08 and 3.27 at the Si and C interfaces in the relaxed initial configuration, respectively, whereas they are 8.58 and 4.55 in the annealed configuration.

Figures 4(a) and 4(b) show the individual BOP and bond length for all interfacial bonds in the relaxed and annealed configurations, respectively. To emphasize the

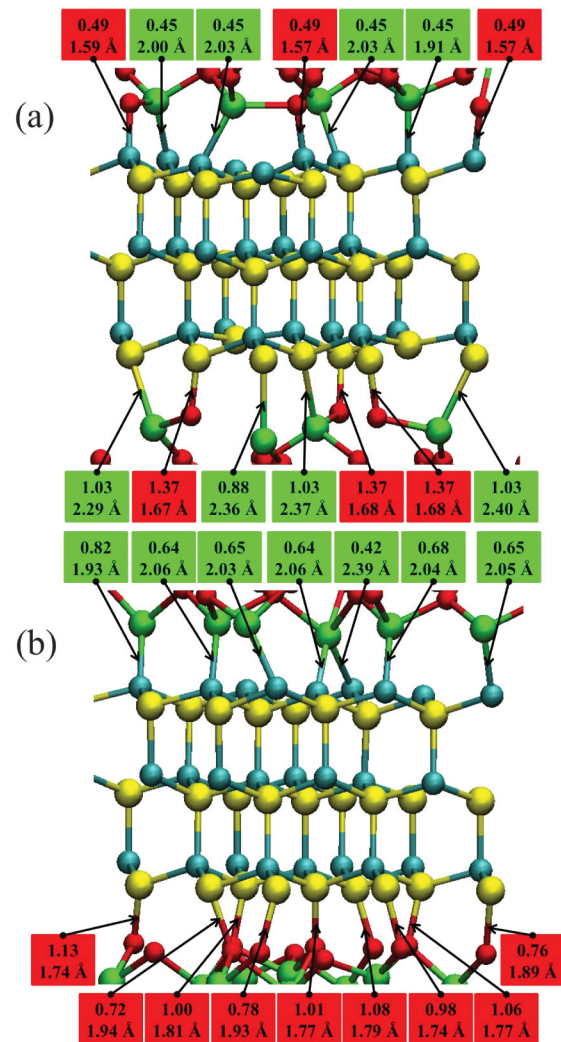


FIG. 4 (color). Snapshots of the relaxed (a) and annealed (b) interfacial structures seen along the $\langle 12\bar{3}0 \rangle$ crystallographic direction of the SiC 3C crystal. The top and bottom numerals for each bond are the bond overlap population and bond length.

bond purification by annealing, each pair of numerals (top and bottom numerals denote the BOP and bond length of the bond, respectively) is highlighted by red or green color for a bond containing O or Al, respectively. At the C interface in the relaxed structure, C-O and C-Al bonds are mixed and two out of nine C atoms do not form bonds with any Al or O atoms as shown in Fig. 4(a). After annealing, C-O bonds disappear and C atoms bond only with Al and Si atoms. Still two C atoms have no bond across the interface [Fig. 4(b)]. While the C-Al bond lengths are almost the same before and after annealing, the value of BOP of each bond becomes larger by annealing (except for one longer bond of length 2.39 Å). As for the Si interface in the relaxed structure, Si-O and Si-Al bonds coexist and two out of nine Si atoms have no bond with any Al or O atoms [Fig. 4(a)]. After annealing, Si-Al bonds vanish and all nine Si atoms at the interface form Si-O bonds [Fig. 4(b)]. By annealing, the length of Si-O bonds becomes longer and the BOP per bond becomes smaller.

Table I summarizes the number of bonds per interfacial unit cell for different types of bonds, along with the average BOP per bond and bond length, at the C and Si interfaces in both relaxed and annealed configurations. After annealing, the Si-terminated SiC surface and Al₂O₃ form a stronger interface (i.e., Si interface) with the Si-O bond density of 12.2 nm⁻² and the average bond length of 1.82 Å, whereas the weaker interfaced formed by the C-terminated SiC surface and Al₂O₃ (i.e., C interface) has a smaller Al-C bond density of 9.46 nm⁻² with a

TABLE I. Summary of the interfacial bonds at the relaxed and annealed interfaces. The number of bonds per interfacial unit cell is shown for different types of bonds, along with the average BOP per bond and bond length, at the C and Si interfaces in both relaxed and annealed configurations.

Relaxed interfaces			
C interface	Number of bonds	Average BOP	Avg. bond length (Å)
C-Al	4	0.45	1.99
C-O	3	0.49	1.58
Si-interface			
Si-Al	4	0.99	2.36
Si-O	3	1.37	1.68
Annealed interfaces			
C interface	Number of bonds	Average BOP	Avg. bond length (Å)
C-Al	7	0.64	2.08
C-O	0
Si-interface			
Si-Al	0
Si-O	9	0.95	1.82

longer average bond length of 2.08 Å. The size effect on the BOP and bond length of individual bonds is found to be small (see Fig. S3 and Table S1 [24]).

We have also studied the effects of interfacial structures on the electronic properties at the interfaces. Figures S4 and S5 [24] show partial electronic densities of states projected onto atomic layers parallel to the interface for the relaxed and annealed configurations. The results demonstrate significant effects of thermal annealing on the interfacial electronic structures, which in turn should have profound impacts on applications such as high-power electronic devices.

The changes of interfacial bonding shown in Fig. 4 and Table I are due to displacements of atoms near the interfaces, which in turn cause structural changes to form interphases. Comparison of Figs. 4(a) and 4(b) shows that the structural changes occur predominantly in the Al₂O₃ side. Figure 5 shows the coordination numbers of Al (circle) and O (square) atoms as a function of the distance from the Al₂O₃/SiC interface. The coordination numbers deviate from the bulk values (6 for Al and 4 for O) at the interfaces. In the case of the weaker C-interface (dashed lines), the Al and O coordination numbers return to the bulk values just in one monolayer (~2 Å) away from the interface, signifying the highly localized interphase. On the other hand, deviation of the coordination numbers from the bulk values at the stronger Si-interface (solid lines) extends over 4 monolayers (~8 Å). This is understandable because the interphase structure is determined by the tradeoff between the energy lowering by strengthened interfacial bonding and the energy increase due to the associated interphase structural deformation [3,4]. Accordingly, the stronger Si interface forms a more extended interphase.

In summary, our high-temperature quantum molecular dynamics simulations of α -Al₂O₃(0001)/3C-SiC (111) interfaces revealed bond purification by thermal annealing,

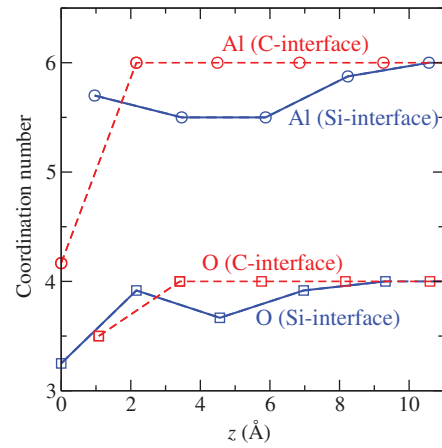


FIG. 5 (color). Coordination numbers of Al (circle) and O (square) atoms as a function of the distance from the Al₂O₃/SiC interface. Solid and dashed lines indicate those at the Si and C interfaces, respectively.

which produces stronger interfaces consisting solely of cation-anion bonds, accompanied by the formation of interphases extending 2–8 Å. Though structural details may depend on the annealing schedule, the well converged and ordered interfaces with bond purification presented here are likely robust features that may be tested experimentally. In addition to the thermal annealing studied here, photochemical annealing has a great potential for creating high-quality films and interfaces in integrated systems, where high temperature is not an option [25]. This process can be simulated by nonadiabatic QMD simulations [26]. Such atomistic understanding may help rational interfacial design for sustainable deployment of high-temperature ceramic composites for energy and other applications such as power generation systems.

This research was supported by the Department of Energy, Office of Science, Basic Energy Sciences, Materials Science and Engineering Division, Grant No. DE-FG02-04ER-46130. The work in Japan was supported by KAKENHI (23104512). The simulations were performed at the University of Southern California using the 20,925-processor Linux cluster at the Center for High Performance Computing and Communications.

-
- [1] A. L. S. Chua, N. A. Benedek, L. Chen, M. W. Finnis, and A. P. Sutton, *Nat. Mater.* **9**, 418 (2010).
- [2] H. A. Bale, A. Haboub, A. A. MacDowell, J. R. Nasiatka, D. Y. Parkinson, B. N. Cox, D. B. Marshall, and R. O. Ritchie, *Nat. Mater.* **12**, 40 (2013).
- [3] S. J. Dillon, M. Tang, W. C. Carter, and M. P. Harmer, *Acta Mater.* **55**, 6208 (2007).
- [4] M. Baram, D. Chatain, and W. D. Kaplan, *Science* **332**, 206 (2011).
- [5] I. Szlufarska, A. Nakano, and P. Vashishta, *Science* **309**, 911 (2005).
- [6] L. P. Ferroni, G. Pezzotti, T. Isshiki, and H.-J. Kleebe, *Acta Mater.* **49**, 2109 (2001).
- [7] T. Ohji, Y.-K. Jeong, Y.-H. Choa, and K. Niihara, *J. Am. Ceram. Soc.* **81**, 1453 (1998).
- [8] R. Suri, C. J. Kirkpatrick, D. J. Lichtenwalner, and V. Misra, *Appl. Phys. Lett.* **96**, 042903 (2010).
- [9] W. Nakao, *Mater. Sci. Forum* **638–642**, 2133 (2010).
- [10] S. Ansell, S. Krishnan, J. Weber, J. Felten, P. Nordine, M. Beno, D. Price, and M.-L. Saboungi, *Phys. Rev. Lett.* **78**, 464 (1997).
- [11] G. Gutierrez, A. B. Belonoshko, R. Ahuja, and B. Johansson, *Phys. Rev. E* **61**, 2723 (2000).
- [12] P. Vashishta, R. K. Kalia, A. Nakano, and J. P. Rino, *J. Appl. Phys.* **103**, 083504 (2008).
- [13] S. Yip, J. Li, M. Tang, and J. Wang, *Mater. Sci. Eng. A* **317**, 236 (2001).
- [14] P. Vashishta, R. K. Kalia, A. Nakano, and J. P. Rino, *J. Appl. Phys.* **101**, 103515 (2007).
- [15] D. R. Clarke, *J. Am. Ceram. Soc.* **70**, 15 (1987).
- [16] D. Marx and J. Hutter, *Ab Initio Molecular Dynamics* (Cambridge University Press, Cambridge, England, 2009).
- [17] P. E. Blochl, *Phys. Rev. B* **50**, 17953 (1994).
- [18] G. Kresse and D. Joubert, *Phys. Rev. B* **59**, 1758 (1999).
- [19] J. P. Perdew, K. Burke, and M. Ernzerhof, *Phys. Rev. Lett.* **77**, 3865 (1996).
- [20] S. G. Louie, S. Froyen, and M. L. Cohen, *Phys. Rev. B* **26**, 1738 (1982).
- [21] J. Ihm, A. Zunger, and M. L. Cohen, *J. Phys. C* **12**, 4409 (1979).
- [22] G. Kresse and J. Hafner, *Phys. Rev. B* **49**, 14251 (1994).
- [23] F. Shimojo, R. K. Kalia, A. Nakano, and P. Vashishta, *Comput. Phys. Commun.* **140**, 303 (2001).
- [24] See Supplemental Material at <http://link.aps.org/supplemental/10.1103/PhysRevLett.111.066103> for a description of simulation methods.
- [25] Y.-H. Kim, J.-S. Heo, T.-H. Kim, S. Park, M.-H. Yoon, J. Kim, M. S. Oh, G.-R. Yi, Y.-Y. Noh, and S. K. Park, *Nature (London)* **489**, 128 (2012).
- [26] W. Mou, S. Ohmura, F. Shimojo, and A. Nakano, *Appl. Phys. Lett.* **100**, 203306 (2012).